ADVANCED FUNCTIONAL MATERIALS
www.afm-journal.de

Realizing an Epitaxial Decorated Stanene with an Insulating Bandgap

Yunyi Zang, Tian Jiang, Yan Gong, Zhaoyong Guan, Chong Liu, Menghan Liao, Kejing Zhu, Zhe Li, Lili Wang, Wei Li, Canli Song, Ding Zhang, Yong Xu, Ke He,* Xucun Ma, Shou-Cheng Zhang, and Qi-Kun Xue*

The exploration of intriguing topological quantum physics in stanene has attracted enormous interest but is challenged by lacking desirable material samples. The successful fabrication of monolayer stanene on PbTe(111) films with low-temperature molecular beam epitaxy and thorough characterizations of its atomic and electronic structures are reported here. In situ angle-resolved photoemission spectroscopy together with first-principles calculations identify two hole bands of p_{xy} orbital with a spin-orbit coupling induced band splitting and meanwhile reveal an automatic passivation of p_z orbital of stanene. Importantly, material properties are tuned by substrate engineering, realizing a decorated stanene sample with truly insulating bulk on Sr-doped PbTe. This finding paves a road for studies of stanene-based topological quantum effects and electronics.

1. Introduction

The great success of graphene research[1,2] has stimulated tremendous effort to search for other innovative 2D materials such as silicene,[3,4] germanene,[5,6] stanene,[7] phosphorene,[8,9] borophene,[10,11] and transition metal dichalcogenides.[12] The prosperous and diverse 2D materials family constitutes an arsenal for exploring new-concept electronic devices as well as fundamental mysteries of condensed matter.[13] A particularly interesting one of them is stanene — a single atomic layer of gray tin (α-Sn) in a honeycomb lattice structure similar to graphene.[14] Different from graphene, stanene is characterized by its structural buckling and large atomic mass which contribute to strong spin-orbit coupling (SOC), offering an ideal platform to explore topology-related physics and electronics.[15] Stanene and its derivatives have been predicted to be 2D topological insulators (TIs)[16,17] with the bulk bandgap up to several hundred meV. Many other exotic properties, including enhanced thermoelectricity,[18] near-room-temperature quantum anomalous Hall effect,[19] and topological superconductivity,[20] are also expected in stanene-based materials, making them useful for various applications ranging from electronics, spintronics to quantum computation.[15]

In a breakthrough experiment in 2015, single-layer stanene was fabricated on Bi_2Te_3(111) by molecular beam epitaxy (MBE),[7] which for the first time proved the existence of this theoretically predicted material. Very recently stanene was prepared on Cu(111) and Ag(111) with an unexpectedly flat structure due to strong coupling with the substrates.[21] All these epitaxial stanene samples, however, are grown on metallic substrates (Bi_2Te_3 has metallic surface states as a TI) and are driven into metallic phases themselves by interaction with the substrates. Transport studies and electronic applications of stanene are only possible in bulk-insulating stanene samples grown on insulating substrates. In this study, we report the first system satisfying this condition, namely bulk-insulating stanene on Sr-doped PbTe(111). Interestingly, the epitaxial stanene in the present experiment is identified to be a decorated stanene, rather than a sheet of bare stanene. The decoration, presumably caused by hydrogen, turns out to be the only option that is consistent with the observed bandgap opening at K/K′ and the corresponding first-principles calculations. The decorated stanene has passivated p_z orbitals and thus is chemically stable in environment, which does not show Dirac-like linear bands

Dr. Y. Zang, Prof. T. Jiang, Y. Gong, Dr. Z. Guan, C. Liu, M. Liao, K. Zhu, Z. Li, Prof. L. Wang, Prof. W. Li, Prof. C. Song, Prof. D. Zhang, Prof. Y. Xu, Prof. K. He, Prof. X. Ma, Prof. Q.-K. Xue
State Key Laboratory of Low Dimensional Quantum Physics
Department of Physics
Tsinghua University
Beijing 100084, P. R. China
E-mail: yongxu@tsinghua.edu.cn; kehe@tsinghua.edu.cn
Prof. L. Wang, Prof. W. Li, Prof. C. Song, Prof. D. Zhang, Prof. Y. Xu, Prof. K. He, Prof. X. Ma, Prof. Q.-K. Xue
Collaborative Innovation Center of Quantum Matter
Beijing 100084, P. R. China
Prof. T. Jiang
College of Optoelectronic Science and Engineering
National University of Defense Technology
Changsha 410073, P. R. China
Prof. Y. Xu
RIKEN Center for Emergent Matter Science (CEMS)
Wako, Saitama 351-0198, Japan
Prof. S.-C. Zhang
Department of Physics
McCullough Building
Stanford University
Stanford, CA 94305-4045, USA
The ORCID identification number(s) for the author(s) of this article can be found under https://doi.org/10.1002/adfm.201802723.

DOI: 10.1002/adfm.201802723

around K/K′ point but displays intriguing low-energy physics around Γ point.[16]

2. Results and Discussion

PbTe is a normal insulator with a bandgap of ≈0.3 eV and the lattice constant in (111) plane close to that of stanene. We prepared PbTe(111) with MBE by co-evaporating Pb and Te to the surface of Bi_2Te_3(111) films on Si(111) (see the schematic of the sample structure in **Figure 1**a). Figure 1b displays the reflective high energy electron diffraction (RHEED) pattern of a 10 bilayer (BL) PbTe(111) film. The clear and sharp diffraction streaks reveal the high crystalline quality of the film. The in-plane lattice constant is estimated to be 4.52 Å. To fabricate epitaxial stanene, we evaporated Sn onto the PbTe(111) films at 150 K and then annealed the sample up to 400 K. Such low growth and annealing temperatures are necessary to avoid diffusion of Sn atoms into PbTe (see Experimental Section for details). After growth of 1 monolayer (ML) Sn, the RHEED streaks (Figure 1c) remain sharp and exhibit no detectable shift in their positions, which suggests perfect epitaxial growth of Sn on PbTe(111). Figures 1d and e display the scanning tunneling microscopy (STM) topographies of PbTe(111) before and after growth of 1 ML Sn, respectively. The evolution of the surface morphology clearly shows 2D growth of Sn on PbTe(111) surface (also see Figure S1, Supporting Information). The depth of the vacancies in the Sn overlayer is 3.6 Å (see the inset of

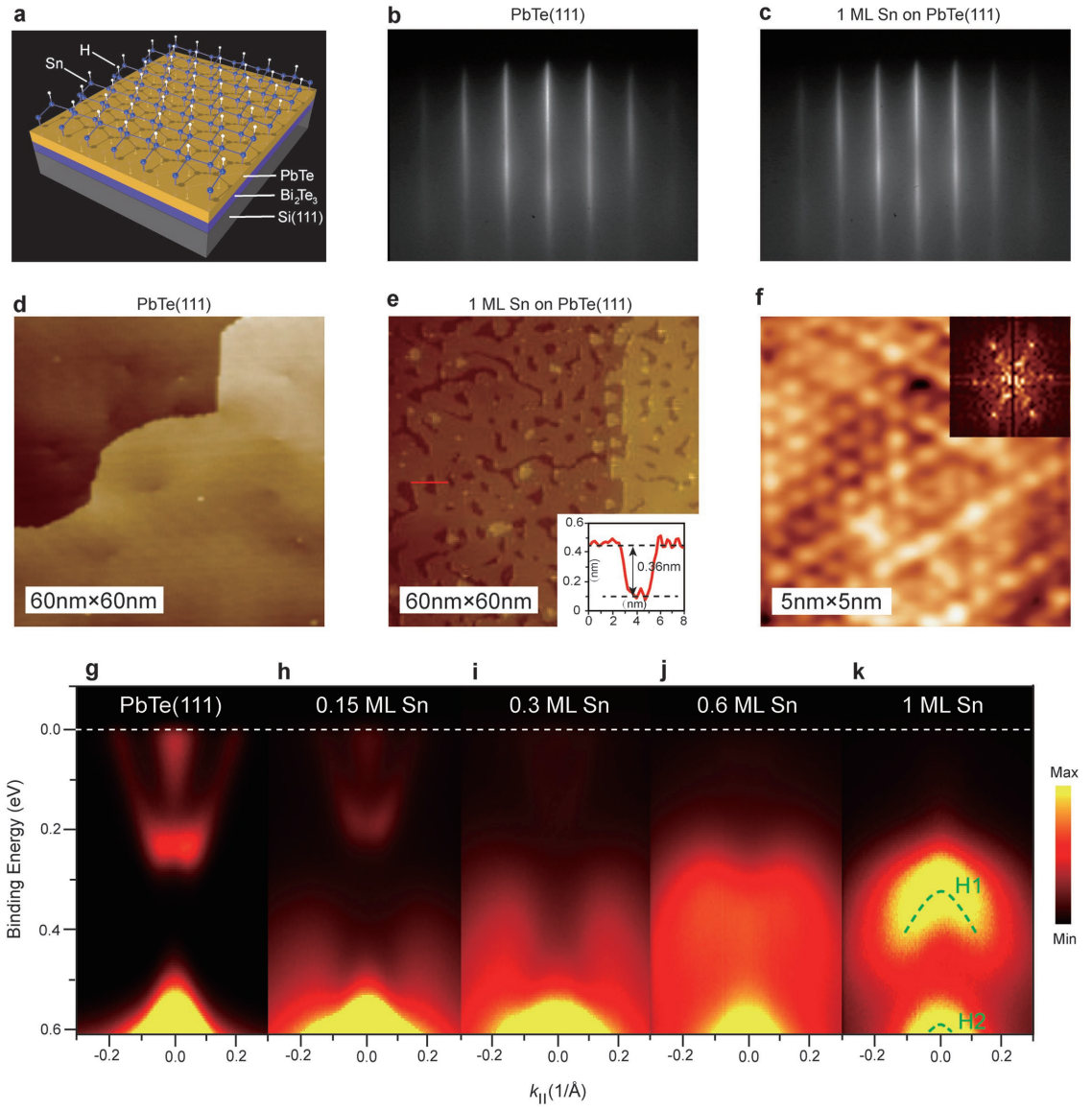

Figure 1. MBE growth of stanene on PbTe(111). a) Schematic of the sample structure. The p_z orbitals of stanene are passivated, possibly by hydrogen. b,c) RHEED patterns of (b) a 10 BL PbTe(111) film and (c) 1 ML Sn grown on a 10 BL PbTe(111) film. d,e) STM images (both 60 × 60 nm) of (d) a 10 BL PbTe(111) film and (e) 1 ML Sn grown on 10 BL PbTe(111) film. The inset of (e) shows the line profile along the red line. f) Atomic-resolution STM of monolayer stanene (scanned at V = 0.7 V, I = 200 pA). The inset of (f) shows the Fourier transformation image. g–k) ARPES bandmaps of Sn grown on PbTe(111) with coverage of (g) 0 ML, (h) 0.15 ML, (i) 0.3 ML, (j) 0.6 ML, and (k) 1 ML around $\bar{\Gamma}$ point, respectively.

Figure 1e) which is consistent with the thickness of single-layer stanene.[7] The atomic-resolution STM image (Figure 1f) and the Fourier transformed image (inset of Figure 1f) illustrate hexagonal arrangement of Sn atoms, consistent with the structure of the upper sublattice of stanene honeycomb lattice.

Figure 1g–k displays a series of angle-resolved photoemission spectroscopy (ARPES) band maps of Sn/PbTe(111) with Sn coverage increasing from 0 to 1 ML around $\overline{\Gamma}$ point of the surface Brillouin zone of PbTe(111) (along cut 1 in Figure S5a, Supporting Information). Similar to the early work,[22] the PbTe(111) film is electron-doped and shows a gap of 0.28 eV with the Fermi level cutting the Rashba spin-split surface states that derive from the bulk conduction bands. With increasing Sn coverage, the PbTe bands fade way, and new features appear and finally evolve into two hole bands at $\overline{\Gamma}$ point (Figure 1k).

Figure 2a shows the ARPES spectra of 1 ML Sn/PbTe(111) around $\overline{\Gamma}$ point with larger energy range. One can clearly identify two hole bands, which are designated as H1 and H2, respectively. H1 band is located at 0.32 eV below the Fermi level and 0.34 eV above H2 band. In the spectra around $\overline{K}$ point (along cut 2 in Figure S5a, Supporting Information), a quite blurred band ≈0.85 eV below the Fermi level can be distinguished if measurement is taken soon after sample preparation (Figure 2b, the second differential spectra are displayed). After the sample is kept in the MBE chamber (base pressure: $\approx 1 \times 10^{-10}$ mbar) for over 2 h, the band cannot be observed anymore (Figure 2c, the second differential spectra are displayed), meanwhile H1 and H2 bands at $\overline{\Gamma}$ point remain almost unchanged. There is no energy band observed between the Fermi level and H1 band, which suggests that the Sn film is insulating with a bandgap of at least 0.32 eV.

To understand the experimental results, we performed first-principles calculations on stanene/PbTe(111) (see details in Experimental Section). As shown in Figure 2d, stanene has a low-buckled honeycomb lattice, constituted by two triangular sublattices stacking together. The p_z orbitals of the bottom sublattice are passivated by the PbTe(111) substrate which was experimentally revealed to be Te-terminated.[22] We found that the ARPES-measured band structure is well reproduced by the calculations if and only if assuming that the p_z orbitals of the upper sublattice are also passivated. For example, when these p_z orbitals are saturated by hydrogen (or halogen) atoms, the calculated band structure includes two hole bands around Γ point, while a sizable bandgap appears at K/K′, which is well

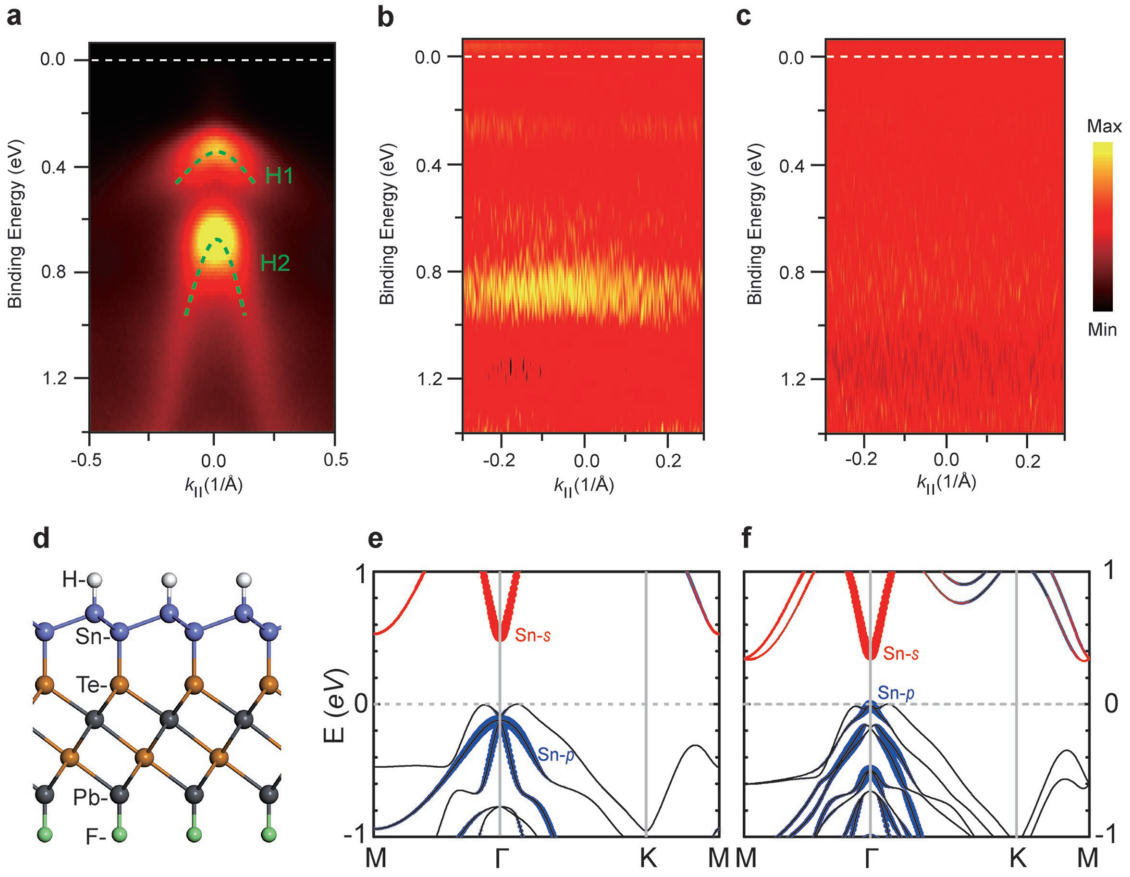

Figure 2. Energy band structure of stanene grown on PbTe(111). a) ARPES bandmap of single-layer stanene epitaxied on PbTe(111) around $\overline{\Gamma}$ point along cut 1 in Figure S5a (Supporting Information). b) ARPES bandmap (second differential data) of as-prepared stanene epitaxied on PbTe(111) around $\overline{K}$ point along cut 2 in Figure S5a (Supporting Information). c) ARPES bandmap (second differential data) of stanene epitaxied on PbTe(111) 2 h after preparation around $\overline{K}$ point along cut 2 in Figure S5a (Supporting Information). d) Atomic model of stanene/PbTe(111). e,f) Calculated band structures of stanene/PbTe(111) (a = 4.52 Å) (e) excluding and (f) including the SOC. Red (blue) color highlights the contributions from Sn-s (Sn-p) orbital, and energy is referenced to the valence band maximum.

consistent with the ARPES observation (Figure 2f). In contrast, if the p_z orbitals of the upper sublattice remain dangling, p_z orbital bands should appear close to the Fermi level around K/K′ point (Figure S2, Supporting Information), which is not observed in the ARPES spectra. The blurred feature observed around K point soon after sample preparation (Figure 2b) might come from the bands of unsaturated p_z orbitals. Therefore, ARPES measurements in combination with first-principles calculations imply an automatic saturation of p_z orbitals of stanene in experiment. Moreover, a clear downwards band shift with time was observed in the normal photoemission spectra ($\mathbf{k}_{//} = 0$) of stanene (Figure S7, Supporting Information), which is consistent with our physical scenario that the stanene sample automatically gets decorated in MBE chamber, presumably caused by hydrogen.

The p_z orbitals of stanene are chemically active and therefore can be easily passivated even under ultrahigh vacuum condition for MBE growth. Assuming that the sticking coefficient of atoms or molecules on stanene is 100%, it takes $\approx 10^4$ s to fully cover the surface under the vacuum of 1×10^{-10} Torr. What kind of chemical saturation groups take effect is mysterious to us. One possible source of passivation is hydrogen, considering that hydrogen (atom or molecule) is ubiquitous and difficult to remove from MBE chambers and material samples.[23] We thus assumed hydrogen passivation in our calculations. Nevertheless, we should emphasize that the calculated band structure is not sensitive to what kind of chemical groups passivate the p_z orbitals (Figure S6, Supporting Information), because the most interesting physic of decorated stanene is contributed by its p_{xy} bands.

In the relaxed geometry (for $a = 4.52$ Å), the calculated Sn–H bond length is 1.74 Å, the same as that in free-standing stanane (i.e., hydrogenated stanene). The binding energy of hydrogen, defined as the energy difference of a hydrogen atom before and after adsorption on stanene/PbTe(111), is ≈3.2 eV per atom, indicating a strong chemical bonding. The buckling of stanene (δ), defined as the height difference between the top and bottom sublattices, is 0.96 Å on PbTe(111), which is close to ≈0.93 Å in both stanene and stanane when using the same lattice constant $a = 4.52$ Å. While δ is insensitive to hydrogenation, it gets enhanced in a compressed lattice. Specifically, the value is 1.14 Å on Bi_2Te_3(111) ($a = 4.38$ Å),[15] significantly larger than 0.85 Å in free-standing stanene ($a = 4.68$ Å) and 0.82 Å in free-standing stanane ($a = 4.72$ Å).[16] The vertical distance between the epitaxial stanene and the topmost Te layer is 3.7 Å, consistent with our STM measurement (3.6 Å).

Theoretically, without SOC, the stanene grown on PbTe(111) introduces one electron band and two hole bands around Γ point, which are mainly contributed by Sn-*s* and Sn-p_{xy} orbitals, respectively (Figure 2e). Noticeably, without SOC, the two p_{xy} hole bands are degenerated at Γ point, and they are split when SOC is turned on (Figure 2f). The two hole bands represent a characteristic feature of stanene[16] which is insensitive to substrate and decoration because of the intactness of in-plane Sn orbitals. They are well consistent with H1 and H2 hole bands observed in ARPES, providing a strong evidence for the existence of single-layer stanene. The calculated hole band splitting at Γ point is 0.49 eV, close to 0.34 eV measured from experiment. According to the calculations, the two characteristic hole bands are further spin-split by Rashba effect (Figure 2f), which was not observed.

As deduced from theory, the energy splitting of the p_{xy} hole bands is determined by SOC and depends weakly on strain effects, which can be tested by experiment. The lattice constant of the epitaxial stanene can be controlled by the thickness of PbTe film. Comparing the RHEED intensity profiles of a 5 and a 10 BL PbTe films, we can observe a shift in the diffraction peaks (**Figure 3**a,b). The estimated surface lattice constants of the 5 and 10 BL PbTe films are 4.46 and 4.52 Å, respectively.[24,25] Stanene always keeps perfect epitaxy with PbTe regardless of its lattice constant. Figure 3c,e shows the ARPES bandmaps of the single-layer stanene films grown on 5 and 10 BL PbTe films, respectively. The band structures of the two samples show no obvious difference despite their different lattice constants. The energy splittings between H1 and H2 bands in the two samples are almost the same (Figure 3d,f), in excellent agreement with theoretical prediction (the calculated splitting changes by less than 0.01 eV). This observation implies that the valence bands of the epitaxial stanene mainly have p_{xy} component, without an *s*–*p* band inversion. It implies that the sample might be a topologically trivial insulator.

Checking the band alignment between the epitaxial stanene and PbTe(111) (see the schematic in **Figure 4**a and the analysis on Figure S3, Supporting Information), we found that the conduction bands of PbTe cover a large portion of the stanene gap. The Fermi level, although lying in the stanene gap, cuts the substrate conduction bands, which is unfavorable for transport studies and electronic applications of stanene. Doping a small amount of Sr in PbTe can significantly increase its bulk gap up to ≈0.7 eV.[26] We prepared Sr-doped PbTe(111) by co-evaporating Sr in MBE growth of PbTe. In the ARPES bandmap of a $Pb_{0.9}Sr_{0.1}Te$(111) film (Figure 4c), the valence band maximum is 0.65 eV below the Fermi level, and no conduction bands are observed, which suggests a truly insulating substrate resulting from bandgap enhancement. The band structure of stanene grown on $Pb_{0.9}Sr_{0.1}Te$(111) is almost the same as that of stanene/PbTe(111). The bulk gap of the epitaxial stanene is now located in the substrate gap (see the schematic in Figure 4b). The stanene/$Pb_{0.9}Sr_{0.1}Te$(111) structure is thus expected to show native properties of stanene in transport measurements.

Although the obtained epitaxial stanene is likely to be a topologically trivial insulator, one can drive it into the 2D TI phase by increasing the film thickness or the lattice constant.[16,27] From the ARPES data of a bilayer and a triple-layer stanene films (Figure S4, Supporting Information and ref. [29]), we observed additional hole bands crossing the Fermi level, which could lead to an *s*–*p* band inversion at higher energy. Further studies are needed to reveal their topological properties. Since the lattice constant of epitaxial stanene can be tuned by the PbTe substrate, by using similar substrate materials with larger lattice constants, such as EuTe, SrTe, BaTe, or their alloys, one may further expand the lattice of epitaxial stanene, driving it into the 2D TI phase.[28]

In multilayer stanene samples, superconductivity was observed and was found to be robust in atmospheric condition.[29] It is because the superconductivity of multilayer stanene is contributed by the chemically stable p_{xy} orbitals and *s* orbitals around Γ point, while the chemically reactive p_z orbitals are passivated, which gives rise to a bandgap around K/K′ point. For a single-layer stanene, the topological properties are also determined by the p_{xy} orbitals and *s* orbitals around Γ point.

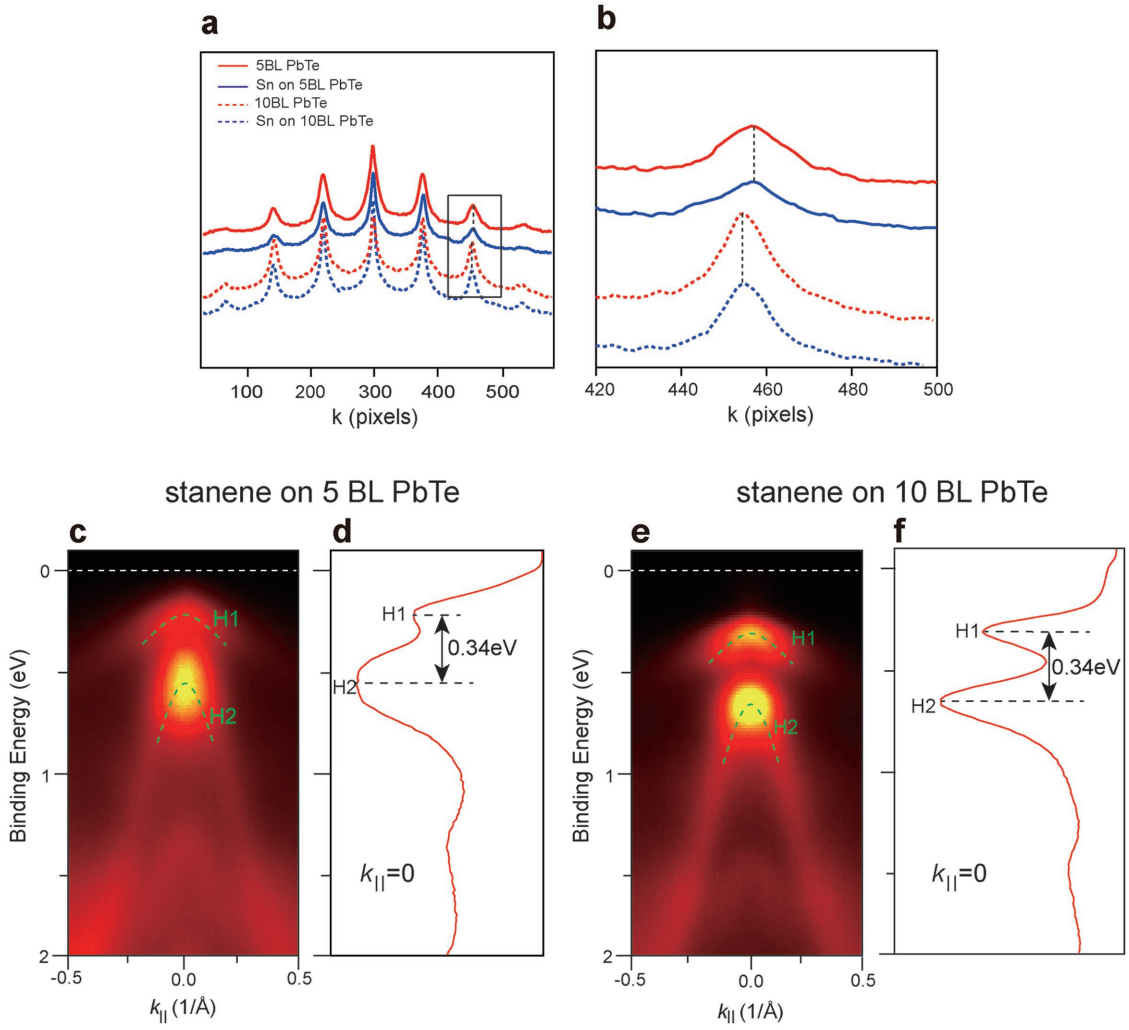

Figure 3. Band structures of the epitaxial stanenes of different lattice constants. a) The intensity profiles of the RHEED patterns of a 5 and a 10 BL PbTe(111) films with and without stanene grown on it. b) A close view of the intensity profiles shown in the black box in (a). c,e) ARPES bandmaps of stanenes grown on (c) 5 BL and (e) 10 BL PbTe(111) films. d,f) Normal photoemission spectra ($k_{//} = 0$) of stanenes grown on (d) 5 BL and (f) 10 BL PbTe(111) films.

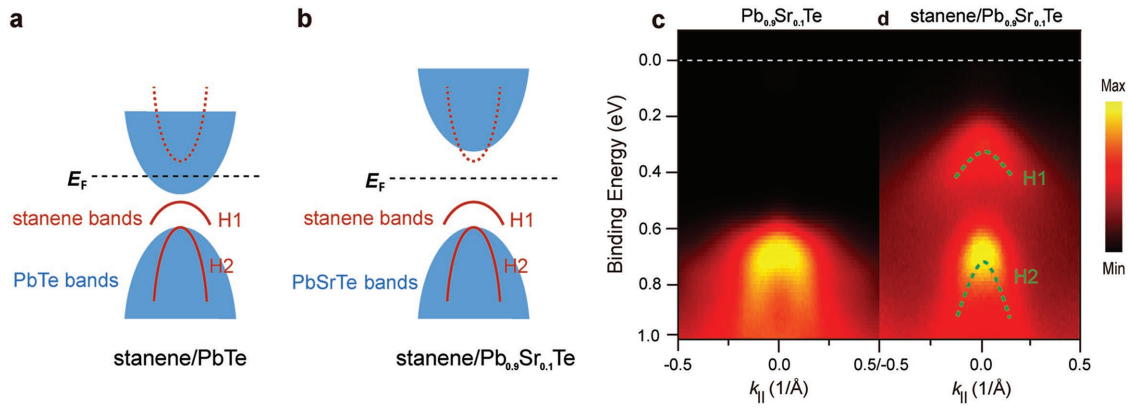

Figure 4. Band structure of stanene grown on Sr-doped PbTe(111). a) Schematic of the band structure of stanene grown on PbTe(111). b) Schematic of the band structure of stanene grown on $Pb_{0.9}Sr_{0.1}Te$(111). c) ARPES bandmap of 10 BL $Pb_{0.9}Sr_{0.1}Te$(111). d) ARPES bandmap of single-layer stanene grown on 10 BL $Pb_{0.9}Sr_{0.1}Te$(111).

Thus, once the 2D TI phase is realized in a decorated single-layer stanene, it is also expected to show stable properties under ambient condition.

3. Conclusion

In summary, we have obtained bulk insulating epitaxial stanene by using Sr-doped PbTe(111) as substrate. Our studies revealed that the p_z orbitals of stanene are automatically passivated even in an ultrahigh vacuum chamber, rendering the properties of decorated stanene insensitive to environment. The realization of stable and truly insulating stanene samples lays a foundation for future experimental studies of various quantum phenomena and electronic applications of stanene.

Note added. After the submission of our work, another group reported a successful fabrication of monolayer stanene on InSb(111), where the epitaxial stanene displays an insulating bandgap.[30]

4. Experimental Section

The experiments were performed in an ultrahigh vacuum system (base pressure: 1×10^{-10} mbar) consisting of MBE (Omicron), STM (Omicron), and ARPES (VG-Scienta) facilities. All the elements were evaporated from standard Knudsen cells. The growth of stanene on PbTe(111) was carried out in a two-step procedure. First, Sn atoms were deposited onto PbTe(111) with the substrate at ≈150 K. And the film was then annealed from 150 to ≈400 K, which improved the film quality. Higher annealing temperature resulted in significant change in the surface morphology and the band structure, probably due to inter-diffusion between Sn and PbTe. The flux of Sn was calibrated by STM (Figure S1, Supporting Information). STM measurements were carried out at 77 K. ARPES measurements were carried out at 90 K with a Scienta R4000 spectrometer and a Gammadata helium discharge lamp (He-Iα, $h\nu = 21.2$ eV).

Computation Methods: First-principles density functional theory calculations were performed by the Vienna ab initio simulation package, using the projector-augmented-wave potential, Perdew–Burke–Ernzerhof (PBE) exchange-correlation functional and planewave basis with an energy cutoff of 400 eV. Stanene/PbTe(111) was modeled by the periodic slab approach using two Pb–Te bilayers with the bottom bilayer fixed and saturated by fluorine for removing the dangling bonds, a vacuum layer of over 12 Å and an $12 \times 12 \times 1$ Monkhorst–Pack k grid. The ultrathin PbTe slab was used to simulate the local chemical bonding of stanene/PbTe(111), which gave a bandgap of PbTe larger than reality, facilitating the analysis of stanene bands. Stanene/PbTe(111) was saturated by hydrogen for fully passivating the p_z orbitals, but the calculated band structure was insensitive to the saturation group (demonstrated in Figure S6, Supporting Information). In contrast, ultraflat stanene on Cu(111) and Ag(111) interacted strongly with the substrate (adsorption energy >1.0 eV per atom),[21] which significantly passivated the p_z orbitals and thus made the material insensitive to the residual gas in experiment. The strain effect applied by the substrate was studied by using different surface lattice constants determined experimentally, $a = 4.46$ and 4.52 Å for 5 and 10 BL PbTe(111) thin films, respectively. The SOC was included in the self-consistent calculations of electronic structure.

Supporting Information

Supporting Information is available from the Wiley Online Library or from the author.

Acknowledgements

This work was supported by the National Natural Science Foundation of China (grant No. 51661135024), Ministry of Science and Technology of China (grant No. 2017YFA0303303), and the Beijing Advanced Innovation Center for Future Chip (ICFC). Y.X. acknowledges support from Tsinghua University Initiative Scientific Research Program and the National Thousand-Young-Talents Program. S.-C. Z. was supported by the U.S. Department of Energy, Office of Basic Energy Sciences, Division of Materials Sciences and Engineering under Contract No. DE-AC02-76SF00515.

Conflict of Interest

The authors declare no conflict of interest.

Keywords

insulating bandgaps, molecular beam epitaxy, stanene

Received: April 21, 2018
Revised: May 23, 2018
Published online: July 1, 2018

[1] A. H. Castro Neto, F. Guinea, N. M. R. Peres, K. S. Novoselov, A. K. Geim, *Rev. Mod. Phys.* **2009**, *81*, 109.
[2] K. S. Novoselov, A. K. Geim, S. V. Morozov, D. Jiang, Y. Zhang, S. V. Dubonos, I. V. Grigorieva, A. A. Firsov, *Science* **2004**, *306*, 666.
[3] P. Vogt, P. D. Padova, C. Quaresima, J. Avila, E. Frantzeskakis, M. C. Asensio, A. Resta, B. Ealet, G. L. Lay, *Phys. Rev. Lett.* **2012**, *108*, 155501.
[4] N. W. Johnson, P. Vogt, A. Resta, P. D. Padova, I. Perez, D. Muir, E. Z. Kurmaev, G. L. Lay, A. Moewes, *Adv. Funct. Mater.* **2014**, *24*, 5253.
[5] M. E. Davila, L. Xian, S. Cahangirov, A. Rubio, G. L. Lay, *New J. Phys.* **2014**, *16*, 095002.
[6] L. Li, S.-Z. Lu, J. Pan, Z. Qin, Y.-Q. Wang, Y. Wang, G.-Y. Cao, S. Du, H.-J. Gao, *Adv. Mater.* **2014**, *26*, 4820.
[7] F. F. Zhu, W. J. Chen, Y. Xu, C. L. Gao, D. D. Guan, C. H. Liu, D. Qian, S. C. Zhang, J. F. Jia, *Nat. Mater.* **2015**, *14*, 1020.
[8] L. Li, F. Yang, G. J. Ye, Z. Zhang, Z. Zhu, W. Lou, X. Zhou, L. Li, K. Watanabe, T. Taniguchi, K. Chang, Y. Wang, X. H. Chen, Y. Zhang, *Nat. Nanotech.* **2016**, *11*, 593.
[9] M. Batmunkh, M. Bat-Erdene, J. G. Shapter, *Adv. Mater.* **2016**, *28*, 8586.
[10] A. J. Mannix, X. F. Zhou, B. Kiraly, J. D. Wood, D. Alducin, B. D. Myers, X. Liu, B. L. Fisher, U. Santiago, J. R. Guest, M. J. Yacaman, A. Ponce, A. R. Oganov, M. C. Hersam, N. P. Guisinger, *Science* **2015**, *350*, 1513.
[11] X. Sun, X. Liu, J. Yu, Y. Li, Y. Hang, X. Zhou, X. Zhou, M. Yu, J. Li, G. Tai, W. Guo, *Adv. Funct. Mater.* **2017**, *27*, 1603300.
[12] Q. H. Wang, K. Kalantar-Zadeh, A. Kis, J. N. Coleman, M. S. Strano, *Nat. Nanotech.* **2012**, *7*, 699.
[13] G. Fiori, F. Bonaccorso, G. Lannaccone, T. Palacios, D. Neumaier, A. Seabaugh, S. K. Banerjee, L. Colombo, *Nat. Nanotech.* **2014**, *9*, 768.
[14] C. Cesare, *Nature* **2015**, *524*, 7563.
[15] A. Molle, J. Goldberger, M. Houssa, Y. Xu, S.-C. Zhang, D. Akinwande, *Nat. Mater.* **2017**, *16*, 163.
[16] Y. Xu, B. H. Yan, H.-J. Zhang, J. Wang, G. Xu, P. Z. Tang, W. H. Duan, S.-C. Zhang, *Phys. Rev. Lett.* **2013**, *111*, 136804.
[17] C.-C. Liu, H. Jiang, Y. G. Yao, *Phys. Rev. B* **2011**, *84*, 195430.

[18] Y. Xu, Z. X. Gan, S.-C. Zhang, *Phys. Rev. Lett.* **2014**, *112*, 226801.
[19] S.-C. Wu, G. C. Shan, B. H. Yan, *Phys. Rev. Lett.* **2014**, *113*, 256401.
[20] J. Wang, Y. Xu, S.-C. Zhang, *Phys. Rev. B* **2014**, *90*, 054503.
[21] J. Deng, A. Zhao, B. Wang, Ultraflat stanene in planar honeycomb structure, to be published.
[22] C. H. Yan, J. W. Liu, Y. Y. Zang, J. F. Wang, Z. Y. Wang, Z.-D. Zhang, L. L. Wang, X. C. Ma, S. H. Ji, K. He, L. Fu, W. H. Duan, Q.-K. Xue, X. Chen, *Phys. Rev. Lett.* **2014**, *112*, 186801.
[23] C. G. Van de Walle, *Phys. Rev. Lett.* **2000**, *85*, 1012.
[24] W. Zhang, R. Yu, H.-J. Zhang, X. Dai, Z. Fang, *New J. Phys.* **2010**, *12*, 065013.
[25] K. Guergouri, R. Triboulet. *J. Cryst. Growth* **1993**, *132*, 20.
[26] D. L. Partin, C. M. Thrush, B. M. Clemens, *J. Vac. Sci. Technol., B* **1987**, *5*, 686.
[27] B.-H. Chou, Z.-Q. Huang, C.-H. Hsu, F.-C. Chuang, Y.-T. Liu, H. Lin, A. Bansil, *New J. Phys.* **2014**, *16*, 115008.
[28] Y. Xu, P. Z. Tang, S.-C. Zhang, *Phys. Rev. B* **2015**, *92*, 081112.
[29] M. H. Liao, Y. Y. Zang, Z. Y. Guan, H. W. Li, Y. Gong, K. J. Zhu, X.-P. Hu, D. Zhang, Y. Xu, Y.-Y. Wang, K. He, X.-C. Ma, S.-C. Zhang, Q.-K. Xue, *Nat. Phys.* **2018**, *14*, 344.
[30] C.-Z. Xu, Y.-H. Chan, P. Chen, X. X. Wang, D. Flototto, J. A. Hleyack, G. Bian, S.-K. Mo, M.-Y. Chou, T.-C. Chiang, *Phys. Rev. B* **2018**, *97*, 035122.